Observation and modeling of single-wall carbon nanotube bend junctions

Jie Han, M. P. Anantram, and R. L. Jaffe
NASA Ames Research Center, Moffett Field, California 94035

J. Kong and H. Dai
Department of Chemistry, Stanford University, Palo Alto, California 94053
(Received 15 December 1997)

Single-wall carbon nanotube (SWNT) bends, with diameters from ~1.0 to 2.5 nm and bend angles from 18° to 34°, are observed in catalytic decomposition of hydrocarbons at 600–1200 °C. An algorithm using molecular dynamics (MD) simulation techniques is developed to model these structures that are considered to be SWNT junctions formed by topological defects (i.e., pentagon-heptagon pairs). The algorithm is used to predict the tube helicities and defect configurations for bend junctions using the observed tube diameters and bend angles. The number and arrangement of the defects at the junction interfaces are found to depend on the tube helicities and bend angle. The structural and energetic calculations using the Brenner potential show a number of stable junction configurations for each bend angle with the 34° bends being more stable than the others. Tight-binding calculations for local density of state and transmission coefficients are carried out to investigate electrical properties of the bend junctions. [S0163-1829(98)05620-3]

I. INTRODUCTION

Recently, Dai *et al.*[1] reported single wall carbon nanotubes (SWNT's) produced by molybdenum-catalyzed decomposition of carbon monoxide at 1200 °C. That work provides the first experimental evidence of SWNT's produced by preformed catalytic particles. It has been shown more recently[2] that similar SWNT production also can be achieved using other catalyst particles and hydrocarbons at 600–1000 °C. Moreover, the isolated SWNT's grown in these processes offer deep insight into some interesting structures. For example, isolated SWNT sharp bends, as shown in Fig. 1, have been frequently observed.[2] Most show clearly defined bend angles of ~18°, 26°, and 34°, with tube diameters between ~1 and 2.5 nm, but the other bend angles might be present.

Individual and bundled SWNT's, grown by arc discharge[3] and laser ablation[4] methods, are also often in bent, coiled, and even seamless toroidal configurations. However, in these cases the continuous variations in the curvatures are different from those in Fig. 1, and attributed to elastic bending. In contrast, complex multiwall nanotube (MWNT) bends are observed as free-standing structures,[5] helices,[6] and L, Y, and T branches,[7] when grown by the arc discharge and catalyst particle methods. These are believed to be nanotube junctions with topological defects, such as pentagon-heptagon pairs, at the joints. A nanotube can be either a semiconductor (S) or a metal (M), depending on its helicity and diameter.[8] Thus, a bend connecting two SWNT's can be a M-M, M-S, or S-S heterojunction. This has stimulated a great deal of interest in proposing SWNT junctions as nanoelectronic devices.[9] The catalyst particle method for growing SWNT's may provide exciting opportunities for making SWNT heterojunctions.

Topological defects change the tube helicity or chiral angle when introduced at the end of a growing nanotube. As a result, a junction connecting two different nanotubes is formed. It is not clear by what mechanisms topological defects are introduced and stabilized in a growing SWNT in the catalyst particle process rather than in the carbon arc or laser ablation processes. However, it seems that physical and/or chemical interactions between MWNT layers or tubes and catalyst particles play a role in the formation of defects and bend structures. This is because sharp bends are observed more frequently in MWNT's (with interlayer interactions) than in SWNT's, and in the catalyst particle methods (with tube-catalyst particle interactions) than in the arc and laser

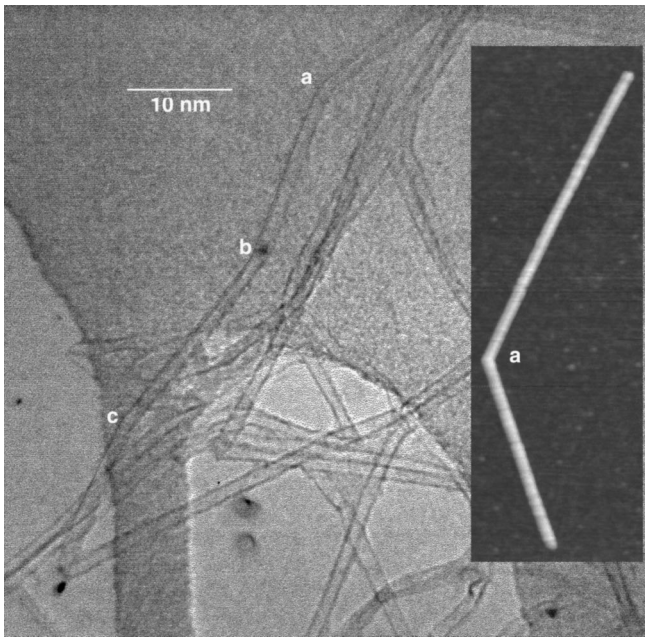

FIG. 1. Representative TEM and atomic force microscopy (AFM) (insert) images of the isolated SWNT bends, grown in catalytic decomposition of hydrocarbons at 600–1200 °C. Three typical bend angles are (a) 34°, (b) 26°, and (c) 18°.

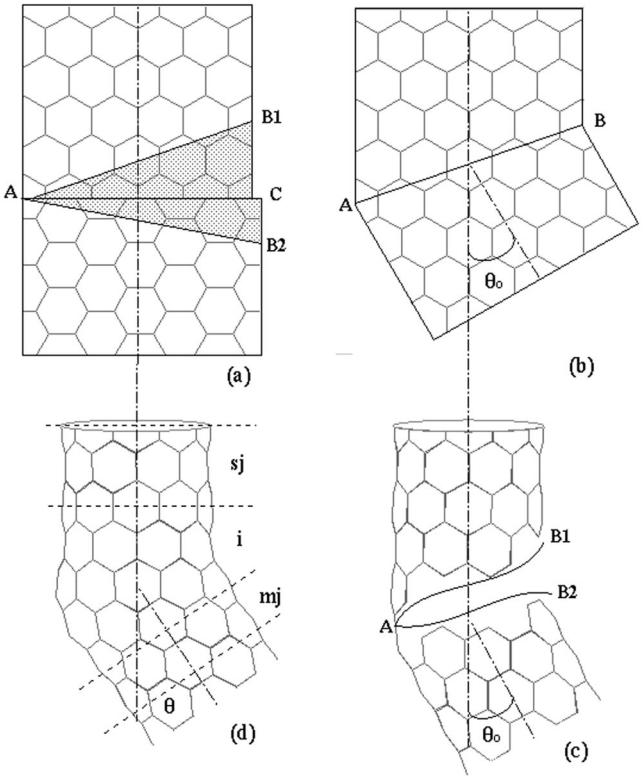

FIG. 2. Construction of a SWNT bend junction (10,0;6,6;36°). (a) and (b), two graphene sheets are connected to form a 30° planar bend; (b) and (c), the planar bend is rolled over to form a 30° tube bend; and (c) and (d), the 30° bend is relaxed to a 36° bend via a MD run. The sj, mj, and i between four broken lines represent the unit cells of two terminal tubes and the junction interface.

methods (with catalysts existing as vapor).[1–6] Some phenomenological growth mechanism models have been proposed for the formation of topological defects and bends on the catalyst particles.[10]

In this work, our goal is to characterize the observed bend structures rather than suggest other mechanisms for their formation. It is possible, but very difficult at present to experimentally determine the tube constituents and the existence of the defects in the observed SWNT bends. Therefore, we use computer modeling tools to explore the possible structural and electrical properties of the observed SWNT bends. The modeling results are expected to help further experimental studies.

II. MODEL CONSTRUCTION

The 30° or small angle (0–15°) bends were modeled by Dunlap[11] and Chico *et al.*,[9] respectively, using a maximally separated and a fused pentagon-heptagon pair along the tube circumference at the joint of two tubes. They did not characterize the observed 18° and 26° bends. In fact, Dunlap's 30° planar bend construction actually models a larger-angle bend as shown below. Therefore, we develop an algorithm to model 0–60° bend junctions using pentagon-heptagon pairs to connect two tubes. This algorithm may be considered to be an extension of Dunlap's constructions.

Figure 2(b) shows a Dunlap 30° planar bend construction that will lead to a bend junction of tubes (10,0) and (6,6). It shows a perfect topological match between two graphene sheets with half-pentagon and half-heptagon at two edges (A and B) of the joint line AB. The 30° tube bend [Fig. 2(c)] is obtained when these two sheets are rolled over. The atoms around the joint line AB in the tube bend, however, are not chemically bonded (the nearest atom distances >1.8 Å) if the chemical bonding (~ 1.42 Å in bond length) in bulk tubes and the 30° bend angle are kept. The straight line AB on the planar sheet is separated into two curves, $AB1$ and $AB2$, on the tube surfaces. In order to chemically bond these atoms, an additional small-angle bending is needed. Thus, the tube bend angle θ [Fig. 2(d)] is larger than the planar bend angle θ_0.

The Dunlap method can be extended to construct other bends, as well. We find that the planar bend angle θ_0 can be related to the helicities of two tubes (m_1,n_1) and (m_2,n_2). That is,

$$\theta_0 = |\phi_1 \pm \phi_2|, \tag{1}$$

$$\phi_i = \tan^{-1}[\sqrt{3}n_i/(2m_i+n_i)], \tag{2}$$

$$d_i = \sqrt{3}a_{c-c}((m_i^2+n_i^2+m_in_i)^{1/2}/\pi), \tag{3}$$

where, ϕ_i and d_i are the chiral angle and diameter of tube (m_i,n_i) and a_{c-c} is the bond length.

Equation (1) shows that the bend angle can be either the sum or the difference of two chiral angles while other possibilities may exist. Thus, a bend following Eq. (1) can have a bend angle from 0 to 60° as the chiral angle of one tube takes values from 0 to 30°. For $\theta_0 = 30°$, the above equations are simplified to Dunlap's relation,[11] after simple triangle function operations on Eqs. (1) and (2):

$$m_2 = n_2(m_1+2n_1)/(m_1-n_1). \tag{4}$$

If $n_1 = 0$, then $m_2 = n_2$. This indicates that a zigzag tube $(n_1,0)$ and an armchair tube (m_2,m_2) always can make up a 30° bend. The junction (10,0)/(6,6) shown in Fig. 2 is one example.

Equation (1) can be used to find the tube helicities, $(m_1,n_1;m_2,n_2)$, in a bend junction for the given bend angle and tube diameters, for example, from the observed images as shown in Fig. 1. Since the four unknowns are related to only three independent equations, we may find a number of tube helicities for the given bend angle and tube diameters.

Giving one set of tube helicities, we follow the steps shown in Figs. 2(a)–2(d) to model a bend junction. A 30° planar bend always can be drawn in a graphene sheet, as shown by Dunlap.[11] The other bends, however, have to start from two graphene sheets, as illustrated in Fig. 2(a). The two sheets are cut by lines $AB1$ and $AB2$, respectively, with $AB1 = AB2$ and $\angle B1AB2 = \theta_0$. The planar bend [Fig. 2(b)] formed in this manner is found to be connected by only pentagon-heptagon pairs in most cases (see Fig. 3), but in some cases also by other types of defects such as four- and eight-member rings, depending on where the sheets are cut and joined. Then the planar bend is rolled over to form the tube bend [Fig. 2(c)]. The tube bend also can be made by creating, cutting, and connecting two straight tubes instead of two sheets. However, we find that two tubes are not topologically matched in this case. In other words, the use of the planar bend construction ensures the right sp^2 bond connections while the planar bend angle is smaller than the actual

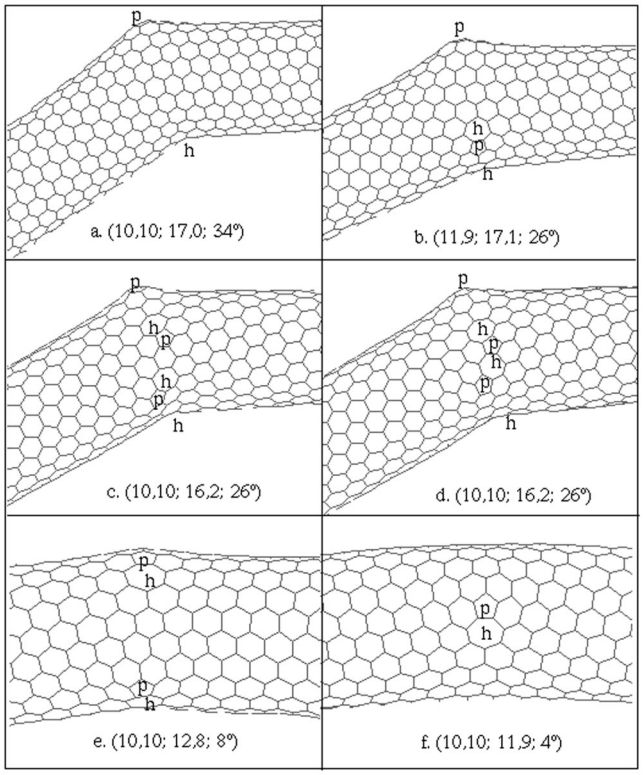

FIG. 3. Examples of simulated SWNT bends. (a): a 34° bend has one pentagon and one heptagon in the opposite sites of the joint; (b)–(d): a 26° bend has three pentagon-heptagon defects with one in opposite sites and the other two defects (fused pentagon-heptagon pairs) in different arrangements; (e) a 8° bend has two fused defects; and (f) a 4° bend has only one fused defect.

tube bend angle. In contrast, directly cutting and joining two tubes may not ensure the bond connections among atoms around the joint interface.

Steps (c)–(d) are performed using a molecular-dynamics (MD) simulation based on the Brenner empirical potential.[12] This potential reliably describes chemical bonding in graphite, and straight and toroidal nanotubes,[13] and therefore allows us to seek stable defect configurations and stable bend structures. The MD simulation is carried out at 1000 °C. At this temperature, the strained tube bends [Fig. 2(c)] quickly change to the relaxed structures [Fig. 2(d)].

Using the above algorithm, we have been able to model and characterize a variety of SWNT bend junctions with the bend angles from ~0 to ~60°. In this present work, we take that $d1 \cong d2 = 1.36\ \text{nm} \pm 3\%$ and $\theta = (18°, 26°, 34°) \pm 1°$ to model the observed SWNT bends. The results are summarized in Table I. The relaxed bend angles and energies were obtained from a energy minimization starting with relaxed structures from the MD simulations.

III. BEND STRUCTURES

It can be seen from Table I that the relaxed bend angles are always larger than the planar bend angles, by roughly 3–4°. The bend angles are ~34, 26, and 18° for the relaxed bends from the initial values of ~30, 23, and 15°, respectively. For smaller diameter tubes, this difference is even larger, about 6–8°, based on our simulations for bend junctions, (6,6)/(10,0), (5,5)/(9,0), (5,5)/(6,4), and (5,5)/(7,3). The difference between the planar bend angle and the tube bend angle was previously explained using Fig. 2. If a tube diameter is large enough, the bend angle does not change much before and after the graphene sheet is rolled over. That is, the difference between the planar bend angle and the tube bend angle decreases with increasing tube diameter. The relaxed tube bend angle also depends on interatomic interactions or the interaction potentials. For example, the bend angles of (9,0)/(5,5) and (10,0)/(6,6) were found to be 40° and 37°, respectively, using a simple empirical potential but only 36° for (9,0)/(5,5) using a semiempirical molecular-orbital calculation.[14]

Now we characterize the SWNT bend structures shown in Table I. A SWNT is described by the tube helicity (m,n) or geometry (d,ϕ). Mechanical and electrical properties of the SWNT have been shown to be a simple function of these structural or topological parameters if the SWNT is defect free, i.e., a perfect carbon hexagonal network. Similarly, a bend junction can be characterized by $(m_1,n_1;m_2,n_2;\theta)$ if these parameters are also related to the atomic structure at the joint interface or the defect configurations at the joint such as the number and arrangement of topological defects. In the following discussion, we define a junction by $(m_1,n_1)/(m_2,n_2)$ and a bend by θ only.

Table I shows the dependence of the bend angle on the number of defect pairs in bend junctions. The numbers of pentagon-heptagon defect pairs required for forming 34, 26, and 18° bends are one, three, and five, respectively. A bend can have different junctions (e.g., a 34° bend has four different junction configurations). A junction also can have two bend angles, $\phi_1+\phi_2$ and $|\phi_1-\phi_2|$, because of the dependence of the bend angle on the numbers of defects. For example, junction (17,1)/(11,9) in Table I has two bend angles, 34° ($\theta_0=\phi_1+\phi_2=29.5°$) and 26°($\theta_0=|\phi_1-\phi_2|=23.9°$). Figure 3 also shows the dependence of the bend angle on the arrangement of defects. One pentagon-heptagon defect pair can lead to a 34° bend junction (10,10)/(17,0) [Fig. 3(a)] or a 4° bend junction (10,10)/(11,9) [Fig. 3(f)] when separated to the opposite sides of the junction or fused at the joint circumference. Similarly, two defect arrangements can result in a 8° bend junction (10,10)/(12,8) [Fig. 3(e)] if two fused pentagon-heptagon pairs are used, or a 30° bend if one pentagon-heptagon is fused and the other one is separated in the manner as shown in Fig. 3(a). Thus, the same number of defects can lead to different bend angles because of different arrangements of defects at the junction interfaces.

We now give some insight into the defect configurations at the bend junction interface. A common feature to all bends is that the defects are aligned along the joint circumference. A defect can be separated or fused, leading to a larger or a smaller bend angle [e.g., Fig. 3(a) versus 3(f)]. The two arrangements in Figs. 3(a) and 3(f) were originally proposed, respectively, by Dunlap[11] and Chico *et al.*[9] All the bends in Table I are found to be formed only by one of these types of pentagon-heptagon pairs, as illustrated in Fig. 3. Thus, a fused and a maximally separated defect along the joint circumference are the basic construction units and the common features of the bend junctions. Starting from a 34° bend with a maximally separated defect [Fig. 3(a)], addition of fused

TABLE I. Structures and energetics of simulated SWNT bend junctions.

$(m_2,n_2)/(m_1,n_1)$	d_2/d_1 (nm)	ϕ_2/ϕ_1, °	ϕ_0, °	eV/atom	junction
Junctions to reach a relaxed 34° bend (one defect, i.e., one pentagon-heptagon pair)					
(17,0)/(10,10)	1.331/1.356	0.0/30.0	30.0	−7.3134	S/M
(17,1)/(11,9)	1.372/1.358	2.8/26.7	29.5	−7.3139	S/S
(16,2)/(12,8)	1.338/1.365	5.8/23.4	29.2		S/S
(15,4)/(13,6)	1.358/1.317	11.5/18.0	29.5	−7.3126	S/S
Junctions to reach a relaxed 26° bend (three defects)					
(17,0)/(12,8)	1.331/1.365	0.0/23.4	23.4	−7.3024	S/S
(17,1)/(13,7)	1.371/1.376	2.8/20.2	23.0		S/M
(17,1)/(11,9)	1.371/1.358	2.8/26.7	23.7	−7.3098	S/S
(16,2)/(13,6)	1.338/1.317	5.8/18.0	23.8		S/S
(16,2)/(10,10)	1.338/1.356	5.8/30.0	24.2	−7.3062	S/M
(16,3)/(14,5)	1.385/1.336	8.4/14.7	23.1		S/M
Junctions to reach a relaxed 18° bend (five defects)					
(17,0)/(14,5)	1.331/1.336	0.0/14.7	14.7	−7.3031	S/M
(17,1)/(13,6)	1.372/1.317	2.8/18.0	15.2		S/S
(16,3)/(12,8)	1.385/1.365	8.4/23.4	15.0	−7.2983	S/S
(15,4)/(11,9)	1.358/1.358	11.5/26.7	15.2		S/S
(14,5)/(10,10)	1.336/1.356	14.7/30.0	15.3	−7.3014	M/M

defects leads to a smaller bend angle [Figs. 3(b)–3(d)]. In contrast, from the 4° bend with one fused defect, adding more fused defects results in a larger bend [Fig. 3(e)].

There may be a number of defect configurations for two or more fused defects in a bend junction. For example, the bend junction, (10,10;16,2;26°), has two fused defects separated [Fig. 3(c)] or fused [Fig. 3(d)] at one side of the joint interface. The two defects separated by one hexagon in Fig. 3(c) also can be separated further, as shown in Fig. 3(b) where two fused pentagon-heptagon defects are arranged in the opposite sites at the joint interface.

The above show that the atomic structures of a bend junction, including defect configurations and tube helicities, can be predicted if the bend angle and tube diameters are measured from the observed images. The tube helicities and the bend angle can be used to characterize a bend junction structure as it is related to the number and arrangement of defects at the joint. All the simulated bends in this work are formed from the maximally separated and/or fused pentagon-heptagon defects. There can be a number of defect arrangements for a given bend junction. Energy minimization is needed for further identification of these structures.

IV. BEND ENERGETICS

All the bends shown in Table I are stable in that the topological defects, once formed in a MD simulation, keep their arrangement upon energy minimization in molecular mechanics calculations. The fifth column in Table I shows the minimized energies per atom for the selected bend configurations with capped ends. The end cap is half of a C_{240} fullerene molecule for a (10,10) tube. For other tubes, it is constructed by distributing six pentagons as uniformly as possible in a hexagonal network. There were about 1000 atoms for each bend model used in the energy minimization calculations. Using a similar molecular mechanics calculation, the binding energy was found to be −7.3482 eV/atom for an infinitely long (10,10) tube, −7.3166 eV/atom for a short (10,10) tube with end caps (926 atoms), −6.9873 eV/atom for fullerene C_{60}, and −7.2145 eV/atom for fullerene C_{240}. We see from Table I that the energies per atom of the various junction models are slightly higher than the (10,10) tube energy.

Comparison based only on energy per atom is not well defined unless the number of atoms, tube diameters, and end cap configurations are identical in the structures because all these factors make the contribution to the total energy. However, one can expect that the bend energy decreases with decreasing number of defects. This can be illustrated for the junction (17,1)/(11,9), shown in Table I. This junction has two bend angles, 34° and 26°. It is found that the 34° bend with one defect is 0.0041 eV/atom more stable than the 26° bend with three defects aligned on one side of joint circumference. Considering that this extra energy is resulted from only two additional defects (10 atoms for one fused pentagon-heptagon), the total energy difference is quite large ($\sim 1000\times 0.0041/2 = 2$ eV/defect relative to two fused hexagons). The larger energy in the 26° bend is found to decrease to 1.7 eV/defect by rearranging the two fused pentagon-heptagon defects to the opposite sites of the joint, as shown in Fig. 3(b). The bend junction (10,10;16,2;26°) can have two types of defect arrangements. The structure shown in Fig. 3(c) is found to be more stable than that in Fig. 3(d), by a total energy difference of 0.42 eV. These confirm that the bend energy decreases with decreasing number of defects and also from fused defects to isolated defects.

It is interesting to explore why all the bend models obtained from our MD simulations have only two types of pentagon-heptagon defects: maximally separated and fused defects. We have carried out accurate nonlocal density-functional theory (b3lyp) calculations for model molecules containing pentagons and heptagons in a hexagonal array.[15]

It is found that the total energy and the optimized geometry prefer two configurations. One is to maximally separate a pentagon-heptagon defect in the joint circumference for formation of a bend junction as shown in Figs. 2(d) and 3(a). The other is to fuse the defect along the tube axis for formation of a straight junction. One pentagon and one heptagon lead to more stable structures when fused together than when separated by a C-C bond or a hexagon. Thus, we believe that the bends with one maximally separated defect are more stable than the other bends. We also calculated the energies of (10,10)/(18,0) (996 atoms) and (10,10)/(11,9) (960 atoms) bends with capped tubes using Brenner potential. The energy was found to be -7.3138 and -7.3129 eV/atom for these two bends with bend angles of 34° and 4°, respectively. This shows no significant energy preference for these two types of bends. In other word, the fused pentagon-heptagon pair is not less stable than an isolated pair, as one might believe. However, this comparison is not based on the same tube constituents and cap configurations and therefore is not conclusive.

It should be mentioned that ~34° bends are indeed observed more frequently than other small angle bends in the experimental images.[11] This may be related to the fact that 34° bends are more stable than other bends. Experimentally it is difficult to detect a smaller sharp bend angle from a transmission electron microscopy (TEM) image. It can be seen from Fig. 3(f) that the 4° bend junction with one fused defect, without atomic structures provided by the simulation, could be identified as merely elastic bending of a SWNT. This problem would be solved if the detailed atomic structures could be directly determined experimentally or the electrical properties could be provided as we expect a significant different in electrical properties between a SWNT and a SWNT junction.

V. ELECTRICAL PROPERTIES OF BEND JUNCTIONS

The electrical properties of a SWNT have been shown to be a function of tube structural parameter (m,n) within one π-electron tight-binding scheme.[8] That is, a SWNT (m,n) is metallic (M) if $(m-n)/3$ is an integer and semiconducting (S) if it is not; and the energy band gap of a semiconducting tube has an inverse dependence on the tube diameter. Thus, a SWNT bend junction, with structural parameters $(m_1,n_1;m_2,n_2;\theta)$, can be a M-M, M-S, or S-S junction. The junction types as classified by the tube helicities are shown in Table I. It must be pointed out that the one π-electron tight binding treatment may not be accurate for smaller-diameter tubes, because of significant σ-π hybridization effects, and the local-density approximation (LDA) may be better. This effect, however, can be ignored for tube diameters larger than 1.0 nm. Therefore, the classification of junction types in Table I should be appropriate.

The electronic properties of the bend junctions with small tube diameters (<0.8 nm) have been studied using local density of state (LDOS) calculations based on the one π-electron tight-binding treatment.[9,14] Our interest is in comparing the LDOS of the larger tube diameter tube junctions with those of smaller ones, and in using transmission coefficients to further understand the electrical properties of the SWNT bend junctions.

We have developed an algorithm to calculate LDOS and transmission coefficients for SWNT junctions using one π-electron tight-binding model and a Green's-function technique within the Landauer formalism. The principle and method of this algorithm are very similar to those previously reported.[9] This algorithm takes the atom configurations of two SWNT unit cells and the arrangement of atoms in the junction interface as inputs, and treats the terminal tubes as infinitely long. In this work, we present the results of these calculations using a hopping parameter of 3.1 eV for junctions (6,6)/(10,0) and (10,10)/(17,0). The unit cells and interfaces are defined in Fig. 2(d) for junction (6,6)/(10,0). One unit cell contains 24 and 40 atoms (mj) for the metallic tubes (6,6) and (10,10), and 40 and 68 atoms (sj) for the semiconducting tubes (10,0) and (17,0), respectively. The interface region i includes an isolated pentagon-heptagon defect, and hexagons along the joint circumference.

The unit-cell averaged LDOS's are shown in Figs. 5(a) and 5(b) for junctions (6,6)/(10,0) and (10,10)/(17,0), respectively. The unit cells denoted by mj and sj $(j=1,2,3,\ldots)$ are further away from the interface for larger values of j. Common features to these two junctions can be seen. The LDOS are most distorted in the interface region, and asymmetric about the Fermi energy of 0 eV. They indicate that the distribution of the unoccupied states is more affected by the presence of the pentagon-heptagon defects than that of the occupied states. Moving away from the interface, the perfect tube DOS features are recovered. The LDOS at unit cells $m3$ and $s4$ show the basic van Hove singularities of the perfect metallic and semiconducting tubes, respectively. These features are basically the same as those previously reported for junctions (6,6)/(10,0) (Ref. 14) and (7,1)/(8,0).[9]

It can be seen from the LDOS at $S(\sim s4)$ and $M(\sim m3)$ that there are more band modes for larger diameter tubes (17,0) and (10,10) than for smaller diameter tubes (10,0) and (6,6) because of more atoms or π electrons per unit cell in the larger diameter tubes. The energy gap is about 1.1 and 0.7 eV for semiconductor tubes (10,0) and (17,0) while a plateau extends about 2.2 and 1.3 eV for metallic tubes (6,6) and (10,10), respectively. This confirms a d^{-1} dependence for the energy gap of semiconducting tubes, and also, interestingly, for the energy plateau width of metallic tubes. The distance from the interface where the semiconductor behavior is recovered is interesting, as well. We cannot see a significant difference in this distance between these two junctions, (6,6)/(10,0) and (10,10)/(17,0) even though the energy gaps in the semiconductor tubes (17,0) and (10,0) and the plateau width in the metallic tubes (10,10) and (6,6) are different. The distance is ~1.4 nm, in agreement with the value (1.5 nm) previously reported for (6,6)/(10,0).[14] In contrast, the distance was found to increase from M/S junction (8,0)/(7,1) to S/S junction (8,0)/(5,3).[9] From these observations, it seems that the distance is more related to defect numbers and arrangements than the energy gap considering that (8,0)/(5,3) contains three defect pairs and the others only one defect pair. In other words, junction interface size is defect dependent. It is also likely that the tight-binding approximation used in this work is not accurate enough to detect the dependence of the transition zone length on the energy gap or the tube diameter.

Figure 4 shows a plot of the transmission coefficient versus energy for SWNT's (6,6) and (10,0) and their junction.

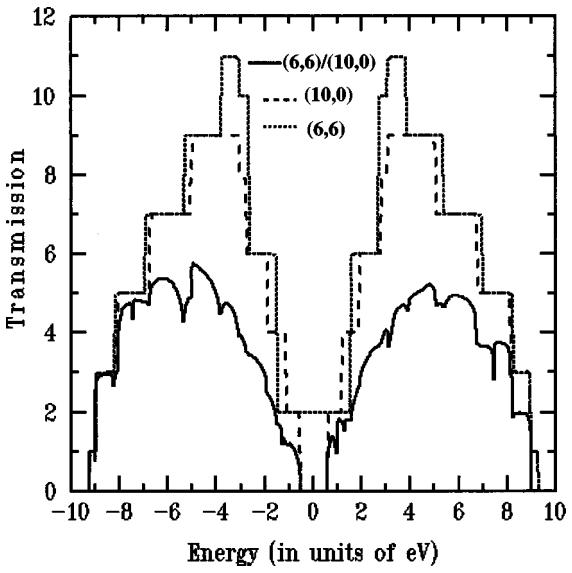

FIG. 4. The transmission coefficient vs energy (eV).

The (6,6) tube has two conducting modes around the Fermi energy and the transmission coefficient increases as new quasi-one-dimensional subbands open (also see LDOS plot, Fig. 5). There is a window of energy around 3.1 eV (also the hopping parameter), where the transmission coefficient is eleven due to the 11 subbands that are open. For larger energies subbands begin to close and so the transmission decreases. The (10,0) tube is a semiconductor (see Fig. 5) and so the transmission coefficient around the Fermi energy is zero. The band gap is about 1.0 eV and for energies away from the gap, subbands open to yield a maximum transmission of 9, after which subbands close, resulting in a decrease in the transmission coefficient. When a M/S junction is formed between the two SWNT's, the transmission coefficient exhibits a gap. This gap is the same as that of the band gap of the semiconducting tube; the semiconducting tube has zero density of states at these energies and so the incident electron from tube (6,6) is fully reflected. For energies outside the gap, the transmission coefficient increases on an average as the number of modes increase. Due to the presence of the barrier at the M/S interface, the transmission coefficient is, however, smaller than that in either the metallic or the semiconducting tube side for all energies. While the transmission coefficient and the DOS of the uniform tubes are symmetric around the Fermi energy, those of the junction are not. The transmission coefficient is smaller for positive energies.

A SWNT bend junction will exhibit the typical heterojunction features of other types of junctions, as shown from LDOS calculations of Chico *et al.*[9] This is further confirmed by our calculations for both the LDOS and transmission coefficients for the observed SWNT junction structures. We are going to use low-temperature STM techniques to measure electrical properties of the observed structures.

VI. CONCLUSION

The SWNT bends, with diameters from ~1.0 to 2.5 nm and bend angles from 18° to 33°, are observed in catalytic

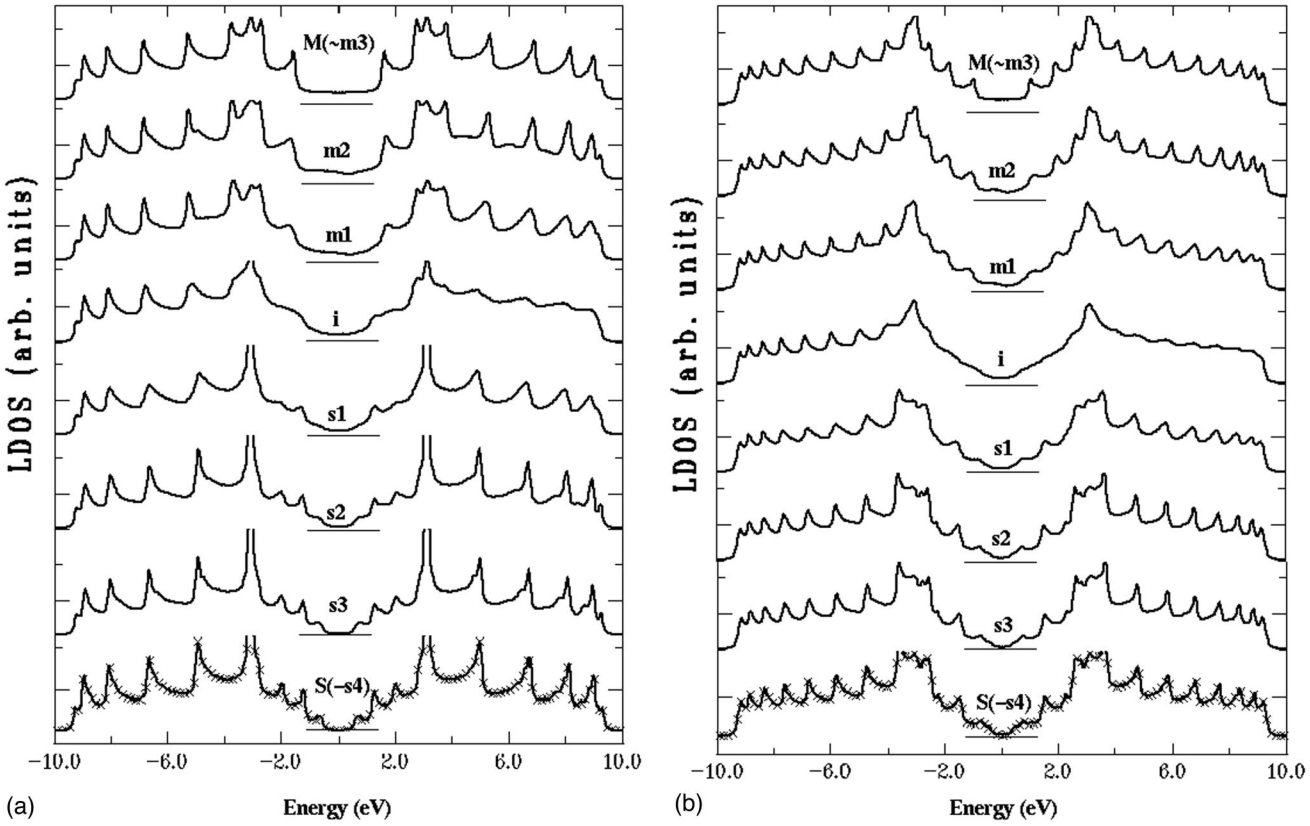

FIG. 5. The unit-cell averaged LDOS vs energy (eV) for junctions (6,6)/(10,0) (a) and (10,10)/(17,0) (b). Solid lines: i interface; and mi and si, unit cells [see Fig. 2(c)]. Cross symbols: perfect semiconducting tubes (10,0) (a) and (17,0) (b).

decomposition of hydrocarbons at 600–1200 °C. These structures are modeled using a new algorithm to connect two SWNT's by introducing pentagon-heptagon defect pairs. It is found that a SWNT bend junction can be characterized by tube helicities and the bend angle. The junction interface structure or the number and arrangement of defects at the interface can be inferred from the tube helicities and bend angle. Structural and energetic calculations using MD and molecular mechanics simulations show a number of stable configurations for the given bend angles and tube diameters. The bend energy decreases from a fused to isolated defect arrangement or with a decrease in defect numbers. The LDOS and transmission coefficient calculations using a tight-binding algorithm suggest that these SWNT bends behave as M/S, M/M, or S/S heterojunctions.

ACKNOWLEDGMENTS

This work was supported by the Director's Discretionary Fund and MRJ, Inc. at NASA Ames Research Center through Contract No. NAS2-14303.

[1] H. Dai, A. Rinzler, P. Nikolaev, A. Thess, D. T. Colbert, and R. E. Smalley, Chem. Phys. Lett. **260**, 471 (1996).

[2] J. Kong and H. Dai (unpublished).

[3] S. Iijima and T. Ichihashi, Nature (London) **363**, 603 (1993); D. S. Bethune, C. H. Klang, M. S. De Vries, G. Gorman, R. Savoy, J. Vazquez, and R. Beyers, *ibid.* **63**, 605 (1993).

[4] A. Thess, R. Lee, P. Nikolaev, H. Dai, P. Petit, J. Robert, C. Xu, Y. H. Lee, S. G. Kim, D. T. Colbert, G. Scuseria, D. Tomanek, J. E. Fischer, and R. E. Smalley, Science **273**, 483 (1996); J. Liu, H. Dai, J. H. Hafner, D. T. Colbert, S. J. Tans, C. Dekker, and R. E. Smalley, Nature (London) **385**, 780 (1997).

[5] N. Koprinarov, M. Marinov, G. Pchelarov, M. Konstantinova, and R. Stefanov, J. Phys. Chem. **99**, 2042 (1995).

[6] S. Amelinckx, X. B. Zhang, D. Bernaerts, X. F. Zhang, V. Ivanov, and J. B. Nagy, Nature (London) **265**, 635 (1994); X. F. Zhang and Z. Zhang, Phys. Rev. B **52**, 5313 (1995).

[7] D. Zhou and S. Seraphin, Chem. Phys. Lett. **238**, 286 (1995).

[8] M. S. Dresselhaus, G. Dresselhaus, and P. Eklund, *Science of Fullerenes and Carbon Nanotubes* (Academic, New York, 1996).

[9] L. Chico, V. H. Crespi, L. X. Benedict, S. G. Louie, and M. L. Cohen, Phys. Rev. Lett. **76**, 971 (1996); L. Chico, L. X. Benedict, S. G. Louie, and M. L. Cohen, Phys. Rev. B **54**, 2600 (1996).

[10] X. B. Zhang, X. F. Zhang, D. Bernaets, G. Van Tendeloo, S. Amelincks, J. Van Landuyt, V. Ivannov, J. B. Nagy, Ph. Lambin, and A. A. Lucas, Europhys. Lett. **27**, 141 (1994); A. Fonseca, K. Hernadi, J. B. Nagy, Ph. Lambin, and A. A. Lucas, in *Carbon Nanotubes*, edited by M. Endo, S. Iijima, and M. S. Dresselhaus (Pergamon, New York, 1996).

[11] B. I. Dunlap, Phys. Rev. B **46**, 1933 (1992); **49**, 5643 (1994); **50**, 8134 (1994).

[12] D. W. Brenner, Phys. Rev. B **42**, 9458 (1990).

[13] J. K. Johnson, B. N. Davidson, M. R. Pederson, and J. Q. Broughton, Phys. Rev. B **50**, 17 575 (1994); D. H. Robertson, D. W. Brenner, and J. W. Mintmire, *ibid.* **45**, 1259 (1992).

[14] Ph. Lambin, A. Fonseca, J. P. Vigneron, J. B. Nagy, and A. A. Lucas, Chem. Phys. Lett. **245**, 85 (1995).

[15] J. Han and R. L. Jaffe, (unpublished).